Dislocation-based model for predicting size-scale effects on the micro and nano indentation hardness of metallic materials

Rashid K. Abu Al-Rub* and Abu N.M. Faruk

Zachry Department of Civil Engineering,
Texas A&M University,
College Station, TX 77843, USA
Fax: +1-979-845-6554
E-mail: rabualrub@civil.tamu.edu
E-mail: nayeem.email@gmail.com
*Corresponding author

Abstract: In micro- and nano-indentation tests for evaluating strength and stiffness properties of engineering materials, a commonly observed phenomenon is the dependence of material properties on the indent size, also known as indentation size effect (ISE). The objective of the present work is to formulate a micro-mechanical based model based on dislocation mechanics for predicting ISE from conical or pyramidal (Berkovich and Vickers) indenters and to compare it with the most widely used Nix-Gao model. The key idea proposed here while deriving the model is a non-linear coupling between the geometrically necessary dislocations (GNDs) and the statistically stored dislocations (SSDs) that eventually allows it to simultaneously predict ISE from both micro- and nano-indentations tests on a wide range of metallic materials while the Nix-Gao model fails to do so. The work also presents a method for identifying the length scale parameter from micro- and nano-indentation experiments and also correlates it with the spacing between dislocations and thus gives a physical interpretation of the material intrinsic length scale.

Keywords: indentation size effect; ISE; micro-indentation; nano-indentation; geometrically necessary dislocations; GNDs; statistically stored dislocations; SSDs; length scale.

Reference to this paper should be made as follows: Abu Al-Rub, R.K. and Faruk, A.N.M. (2010) 'Dislocation-based model for predicting size-scale effects on the micro and nano indentation hardness of metallic materials', *Int. J. Materials and Structural Integrity*, Vol. 4, Nos. 2/3/4, pp.251–277.

Biographical notes: Rashid K. Abu Al-Rub is an Assistant Professor of Civil Engineering at Texas A&M University. He received his BS and MS in Civil Engineering from Jordan University of Science & Technology, and his PhD in Civil Engineering from Louisiana State University. His research interests include computational solid mechanics, size-scale effects, nanocomposites, and constitutive modelling of the inelastic, damage, and fracture behaviour of a wide range of engineering materials.

Abu N.M. Faruk obtained his MS from the Zachry Department of Civil Engineering at Texas A&M University. He obtained his BS from Bangladesh University of Engineering and Technology. His research interests are in size scale effects in small-scale volumes.

1 Introduction

With the emerging area of nanotechnology in recent years, there has been a significant and rapidly growing effort to fabricate small structures in the micro- and nano-metre scales. Along with it came the challenge of evaluating the mechanical properties (e.g., hardness, stiffness, etc.) of materials at these small scales and micro- and nano-indentation tests proved to be the most suitable for their economic as well as fast, precise, and non-destructive merit. However there are numerous indentation tests at scales on the order of a micron or a submicron that have shown that the measured hardness increases significantly with decreasing the indentation size or equivalently the indenter size (e.g., Stelmashenko et al., 1993; De Guzman et al., 1993; Ma and Clarke, 1995; Poole et al., 1996; McElhaney et al., 1998; Lim and Chaudhri, 1999; Elmustafa and Stone, 2002; Gerberich et al., 2002; Swadener et al., 2002; Huber et al., 2002; Abu Al-Rub and Voyiadjis, 2004a). This phenomenon is commonly termed as indentation size effect (ISE).

There are several examples of size effects other than indentation tests. For example, experimental work has revealed that a substantial increase in the macroscopic flow stress can be achieved by decreasing the particle size of particle-reinforced composites while keeping the volume fraction constant (e.g., Lloyd, 1994; Nan and Clarke, 1996; Kiser et al., 1996), by decreasing the diameter of thin wires in micro-torsion test (Fleck et al., 1994), and with decreasing the thickness of thin films in micro-bending test (Stolken and Evans, 1998; Shrotriya et al., 2003; Haque and Saif, 2003). None of these cases of dependence of mechanical response on size could be explained by the classical continuum mechanics, whereas gradient plasticity theory has been successful in addressing the size effect phenomena [see the book by Voyiadjis and Abu Al-Rub (2009) for a detailed review of gradient plasticity theory]. This is due to the incorporation of a micro-structural length scale parameter in the governing equation of the deformation description. Gradient plasticity theory attributes ISE to the evolution of the so-called geometrically necessary dislocations (GNDs) beneath the indenter, which gives rise to strain gradients (Ashby, 1970; Arsenlis and Parks, 1999)

However, the full utility of the strain gradient plasticity theories hinges on one's ability to determine the constitutive length scale parameter, ℓ, which scales the gradient effect. The study of Begley and Hutchinson (1998), Yuan and Chen (2001), Abu Al-Rub and Voyiadjis (2004a, 2004b), and Abu Al-Rub (2007) indicated that micro- and nano-indentation may be the most effective test for measuring the length scale parameter. However, the physical origin of ℓ based on dislocation mechanics has not been discussed until the work of Abu Al-Rub and Voyiadjis (2004a, 2004b). In fact, Abu Al-Rub and Voyiadjis (2004a, 2004b) have shown based on dislocation mechanics that ℓ is proportional to the average spacing between dislocations (or the mean free path for dislocation motion). This met to a great extent the phenomenological arguments by Nix and Gao (1998) and Gao et al. (1999) that ℓ may be interpreted physically as the square of dislocation spacing over the magnitude of the Burgers vector. However, they proposed an expression for ℓ as a function of the magnitude of the Burgers vector multiplied by square of the ratio of the shear modulus to the yield strength and other empirical parameters. This expression yields a constant value for ℓ for a specific material and is independent of the material micro-structural features. Whereas, the studies of Abu Al-Rub and Voyiadjis (2004a) and Voyiadjis and Abu Al-Rub (2005) have indicated that this length scale parameter is not a constant for a given material but since it depends on

the spacing between dislocations is deformation dependent. In other words, as the plastic strain increases, the smaller is the length scale and the weaker is the size effect. Also, Voyiadjis and Abu Al-Rub (2005) proposed a phenomenological expression for ℓ in terms of:

a the average grain size in polycrystalline materials or the particle size in composite materials with dispersed hard particles

b the geometric characteristic size such as the thickness of a thin film, radius of a thin wire, or inter-particle spacing in particulate composites

c the magnitude of the plastic strain

d the rate of strain-hardening (annealed versus work-hardened or pre-deformed materials).

By considering the GNDs generated by a conical indenter, Nix and Gao (1998) utilised the dislocation arguments set by Stelmashenko et al. (1993) and Ma and Clarke (1995) and developed an ISE model that suggests a linear dependence of the square of the micro-hardness to the inverse of the indentation depth. Swadener et al. (2002) utilised the basic precepts given by Nix and Gao (1998) for a conical indenter and developed an ISE model for spherical indenters which suggests a linear dependence of the square of the micro-hardness to the inverse of the diameter of the spherical indenter. However, recent micro- and nano-indentation results show that the predictions of the Nix and Gao (1998) and Swadener et al. (2002) models deviate significantly from the experimental results at small indentation depths (i.e., nano-indentation) in the case of Berkovich and Vickers indenters (e.g., Lim and Chaudhri, 1999; Saha et al., 2001; Elmustafa and Stone, 2002; Feng and Nix, 2004; Abu Al-Rub and Voyiadjis, 2004a; Manika and Maniks, 2006; Abu Al-Rub, 2007) and at small diameters for the case of spherical indenters (Swadener et al. 2002; Abu Al-Rub and Voyiadjis, 2004a). Moreover, Elmustafa and Stone (2002) observed that when the Nix-Gao model is used to fit the experimental results of micro- and nano-hardness, the data at deep indents (micro-hardness) exhibits a straight-line behaviour whereas for shallow indents (nano-hardness) the slope of the line severely changes, decreasing by a factor of ten, resulting in a bilinear behaviour and, therefore, two different values for the material length scale are used to fit the micro- and nano-indentation data. Recently, Huang et al. (2006) modified the Nix-Gao model by reducing the density of GNDs at small indentation depths where two values for the material length scale are also used to fit the micro- and nano-indentation data. Therefore, Nix-Gao model can fit well either the hardness data from micro-indentation or nano-indentation tests, but not both simultaneously. This is a the focus of the present paper where an attempt is made to formulate an ISE model that can accurately and simultaneously predict the micro-hardness and nano-hardness from micro-indentations and nano-indentations, respectively.

Different researchers have addressed this limitation in Nix-Gao model in their works and proposed different measures of remedy. Yuan and Chen (2001), Qui et al. (2001), and Swadener et al. (2002) have modified the Nix-Gao model by incorporating the effect of intrinsic lattice resistance or friction stress. However, it is shown by Huang et al. (2006) and Abu Al-Rub (2007) that the inclusion of the friction stress gives better predictions than the Nix-Gao model but still is not satisfactory to give well predictions of the nano-indentation results. Moreover, Xue et al. (2002) and Qu et al. (2004) have

attributed the deviation of the Nix-Gao model from nano-indentation hardness data to the rounded shape of conical or pyramidal indenter real tips, and therefore, Alkorta et al. (2006) refined the Nix-Gao model by taking into account the tip roundness. However, it is shown in Huang et al. (2006) that the indenter tip radius effect alone cannot explain the nano-ISE especially for 100 nm indents and higher. Zhao et al. (2003) further refined the Nix-Gao model by considering the non-uniform distribution of GND density underneath the indenter but yielded qualitatively the same behaviour as Nix-Gao model with the nano-indentation hardness is over predicted. Feng and Nix (2004) and Durst et al. (2006) reformulated the Nix-Gao model by assuming that the GNDs are stored within the plastically deformed zone of size greater than the contact radius of indentation, which is somewhat similar to the modification proposed by Huang et al. (2006). However, it is shown by Abu Al-Rub (2007) that this modification only affects the value of the material length scale and still suffers from the overestimation of the nano-indentation hardness. Therefore, all of the aforementioned remedies to the Nix-Gao ISE model gave a marginal improvement to the predictions of nano-indentation hardness data such that none of the aforementioned modified models could be used to predict both micro- and nano-indentation results satisfactorily. Recently, Abu Al-Rub (2007) argued that the most likely impediment in the Nix-Gao model is the assumption that the densities of GNDs and SSDs in the Taylor's hardening law are summed arithmetically such that it overestimates the total dislocation density underneath the indenter. He has concluded that a better assumption is to postulate the arithmetic sum of shear stresses from SSDs to that from GNDs and this assumption can yield much better predictions of both micro- and nano-hardness simultaneously. This conclusion is further and thoroughly investigated in this paper.

The present study sheds some insight on the interpretation of the ISE encountered in micro- and nano-hardness from conical or pyramidal indenters and proposes an ISE analytical model that *can predict equivalently well the micro- and nano-indentation hardness data* from conical/pyramidal indentation. This model assesses a non-linear coupling between the densities of SSDs and GNDs in the Taylor's hardening law as argued by Abu Al-Rub and Voyiadjis (2004a, 2004b) and Abu Al-Rub (2007). The predictions of this model are compared to that by Nix and Gao (1998) against a comprehensive set of micro- and nano-indentation tests on several metallic materials. Values for the material length scale parameter are calculated and it is shown that these values vary with the plastic strain for a certain material which is pre-deformed at several plastic strain levels.

2 Physical interpretation of the material length scale

It is assumed, in general, that the total dislocation density represents the total coupling between two types of dislocations which play a significant role in the hardening mechanism. Material deformation in metals enhances the dislocation formation, the dislocation motion, and the dislocation storage. The dislocation storage causes material hardening. The stored dislocations generated by trapping each other in a random way are referred to as statistically stored dislocations (SSDs), while the stored dislocations that relieve the plastic deformation incompatibilities within the polycrystal caused by non-uniform dislocation slip are called GNDs. Their presence causes additional storage of defects and increases the deformation resistance by acting as obstacles to the SSDs

(Arsenlis and Parks, 1999). Therefore, as far as the experimental findings up to day, one cannot assume that GNDs are similar to SSDs since both are different in nature. The SSDs are believed to be dependent on the effective plastic strain, while the density of GNDs is directly proportional to the gradient of the effective plastic strain (Ashby, 1970). Moreover, non-vanishing net Burgers vector from the excess of dislocations of one sign in any region bounded by a closed curve implies the existence of GNDs (Nye, 1953; Arsenlis and Parks, 1999). Therefore, an easy way to distinguish if the material possesses GNDs is by computing the net Burgers vector. SSDs conserve the net Burgers vector of the volume in which they occur, whereas the divergence of dislocation density flux leads to a net change in the Burgers vector of the volume. For more details about different interpretations of the physical nature and properties of SSDs and GNDs the reader is referred to the complete issue in *Scripta Materialia* (Needleman and Gil, 2003).

The densities of SSDs and GNDs can be combined in various ways for which there is little guidance from dislocation mechanics. Mughrabi (2001) concluded that the simple superposition of the density of GNDs on the density of SSDs is *not well founded* and they are unambiguously related. Abu Al-Rub and Voyiadjis (2004a) and Abu Al-Rub (2007) have concluded that the most likely impediment in the Nix and Gao (1998) ISE model in predicting nano-hardness equally as micro-hardness is due to the assumption that the total dislocation density in the Taylor's hardening law is a simple arithmetic sum of both SSD and GND densities. Therefore, Abu Al-Rub and Voyiadjis (2004a, 2004b), Voyiadjis and Abu Al-Rub (2005), and Abu Al-Rub (2007) presented different phenomenological forms to enhance the non-linear coupling between SSDs and GNDs and showed that the discrepancy in the Nix-Gao model predictions of nano-hardness can be largely corrected by incorporating this non-linear coupling. One possible coupling can be assessed by writing the overall flow stress, σ, as follows:

$$\sigma = \left[\sigma_S^{\beta} + \sigma_G^{\beta} \right]^{1/\beta} \tag{1}$$

where σ can be set equal to the effective (or equivalent) stress, for example, $\sigma = \sqrt{3 s_{ij} s_{ij} / 2}$ in case of von-Mises type plasticity, where $s_{ij} = \sigma_{ij} - \frac{1}{3}\sigma_{kk}\delta_{ij}$ is the deviatoric part of the Cauchy stress tensor σ_{ij} with δ_{ij} is the Kronecker delta. The interaction coefficient β is considered as a material constant and used to assess the sensitivity of predictions to the way in which the coupling between the SSDs and GNDs is enhanced during the plastic deformation process. Thus, different values of β implies changes in the strain history. The general form in equation (1) ensures that $\sigma \to \sigma_S$ whenever $\sigma_S >> \sigma_G$ (i.e., classical plasticity) and that $\sigma \to \sigma_G$ whenever $\sigma_S << \sigma_G$. The stresses σ_S and σ_G are associated respectively with the densities of SSDs and GNDs through the Taylor's hardening law as follows:

$$\sigma_S = m\alpha G b\sqrt{\rho_S} \ , \ \sigma_G = m\alpha G b\sqrt{\rho_G} \tag{2}$$

where m is the Taylor factor, which acts as an isotropic interpretation of the crystalline anisotropy at the continuum level; $m = \sqrt{3}$ for an isotropic solid and $m = 3.08$ for FCC polycrystalline metals (Taylor, 1938), G is the shear modulus, b is the magnitude of Burgers vector, and α is a statistical coefficient between 0.1 and 0.5. The empirical

constant α accounts for the strength deviation from regular spatial arrangements of the SSD and GND populations. For impenetrable forest dislocations, Kocks (1966) assumed $\alpha = 0.85$ for SSDs and Busso et al. (2000) assumed $\alpha = 2.15$ for GNDs. For simplicity, in the present work it is assumed that α is the same for both SSDs and GNDs.

Substituting equations (2) into equation (1), one can express the total dislocation density, ρ_T, as follows:

$$\rho_T = \left[\rho_S^{\beta/2} + \rho_G^{\beta/2} \right]^{2/\beta} \tag{3}$$

such that the flow stress σ can be rewritten as:

$$\sigma = m\alpha Gb\sqrt{\rho_T} \tag{4}$$

It is noteworthy that equations (3) and (4) imply that SSDs and GNDs are similar in nature concerning their properties, but the processes of their nucleation, motion, storage, and annihilation are different. The SSDs' density evolves through Burgers vector-conserving reactions based on dislocation mechanics while the GNDs' density evolves due to the divergence of dislocation fluxes associated with the inhomogeneous nature of plasticity in crystals (Arsenlis et al., 2004; Abu Al-Rub and Voyiadjis, 2006). It is believed that SSDs are generated first and then some of these SSDs become geometrical (mainly at grain boundaries and interfaces) and others are trapped due to interaction with obstacles or other dislocations (statistical or geometrical). Therefore, both SSDs and GNDs increase/decrease in density as deformation progresses and both contribute to material hardening. Moreover, the evolution of GNDs does not necessarily increase the total dislocation density. It may also decrease the total density. Whether dislocation density is accumulated or lost due to the flux divergence depends on the participation of the relative densities to the plastic deformation across the volume and on the sign of their divergence. For example, if positive edge dislocations are the only ones within a volume and the plastic strain field is such that more edge dislocations leave the volume than enter the volume, the total dislocation density in the volume will decrease as a result of the inhomogeneous plastic deformation (Arsenlis et al., 2004). However, fundamental research at the discrete dislocation level using the principles in dislocation mechanics is needed for the proper physical interpretation of the evolution and interaction between SSDs and GNDs.

Recently, Abu Al-Rub (2007) has confirmed the conclusions of Abu Al-Rub and Voyiadjis (2004a) that the ideal assumption made by Nix and Gao (1998) in formulating their ISE model of all obstacles being equally strong and equally spaced such that $\rho_T = \rho_S + \rho_G$ is the main reason for the Nix-Gao model not being able to well predict the micro- and nano-hardness simultaneously. Abu Al-Rub (2007) has shown that the real situation in experiments suggests that ρ_T cannot be taken as a simple sum of the densities of SSDs and GNDs and that the total dislocation density under indentation is larger than this simple sum. In fact, for $\beta < 2$ in equation (3), ρ_T is larger than the arithmetic sum of SSD and GND densities, whereas for $\beta > 2$, ρ_T is smaller than the sum. Therefore, β either increases the effect of both kinds of dislocations or decreases such effect. However, Ashby (1970) has pointed out that in general the presence of GNDs will accelerate the rate of SSDs' storage and that an arithmetic sum of their densities

gives a lower limit on ρ_T, which implies that β should be less than 2. Abu Al-Rub (2007) concluded after analysing several nano-indentation data that $\beta \approx 1$ in equation (3). Hence, by setting $\beta = 1$ in equation (1), one can rewrite the total flow stress as a simple arithmetic sum of the flow stresses from SSDs and GNDs, such that:

$$\sigma = \sigma_S + \sigma_G \tag{5}$$

This along with equation (3) which leads to a coupling between SSD and GND densities of the form:

$$\rho_T = \left[\sqrt{\rho_S} + \sqrt{\rho_G}\right]^2 \tag{6}$$

which differs from the linear coupling of the form:

$$\rho_T = \rho_S + \rho_G \tag{7}$$

adopted in formulating the Nix-Gao model. Equation (6) gives a total dislocation density larger than that given by equation (7). Therefore, one concludes that the Nix-Gao model underestimates the total dislocation density. In the following subsequent developments, equations (5) and (6) will be utilised to formulate an ISE model and in exploring the physical origin of the material length scale parameter responsible for the observed size-scale effects.

Plastic strain gradients play an essential role in the prediction of size-scale effects in the deformation behaviour of metals at the micron and submicron scales. The classical plasticity theory, which inherently includes no material length scale, cannot predict size effects. Strain gradient plasticity theories extend the classical plasticity models by explicitly including an intrinsic material length scale and by including the history effects of the surrounding material points on the material point under consideration (i.e., non-locality), and are therefore appropriate for materials and structural systems involving small dimensions. Motivated by the Taylor law in equation (1) at the micro-mechanical level, one can therefore assume the following power-law of the corresponding gradient-dependent flow stress at the mesoscale (Abu Al-Rub and Voyiadjis, 2004a):

$$\sigma = \sigma_{ref}\left(\widehat{\varepsilon}^p\right)^{1/n} \text{ with } \widehat{\varepsilon}^p = \left[\sqrt{\varepsilon^p} + \sqrt{\ell\eta}\right]^2 \tag{8}$$

where σ_{ref} is the reference stress which is a measure of the yield stress in uniaxial tension, ℓ is the material length scale which its physical meaning and origin will be explored in the following development, $n \geq 1$ is the strain-hardening exponent, $\widehat{\varepsilon}^p$ and ε^p are the non-local and local effective (equivalent) plastic strains, respectively, η is an effective measure of the gradient of plastic strain which is related to the GND density. For example, one can assume $\eta = \sqrt{\nabla\varepsilon^p.\nabla\varepsilon^p}$, where ∇ is the first gradient operator. For other expressions of η, one can consult Abu Al-Rub and Voyiadjis (2004a, 2004b). Note that the expression in equation $(8)_2$ is motivated by the expression in equation (6) for the total dislocation density. Therefore, $\widehat{\varepsilon}^p$ represents a measure of the total dislocation density at the mesoscale.

During plastic deformation, the density of SSDs increases due to a wide range of processes that leads to production of new dislocations. Those new generated dislocations travel on a background of GNDs which act as obstacles to the SSDs. If L_S is the average distance travelled by a newly generated dislocation, then the rate of accumulation of strain due to SSDs scales with $\dot{\varepsilon}^p \propto L_S b \dot{\rho}_S$ (Orowan, 1948) such that for proportional loading and monotonically increasing plasticity, one can express ε^p in terms of ρ_S (Abu Al-Rub and Voyiadjis, 2004a, 2004b):

$$\varepsilon = \frac{1}{m} bL\rho \tag{9}$$

Ashby (1970), Arsenlis and Parks (1999) and Gao et al. (1999) showed that gradients in the plastic strain field are accommodated by the GND density, ρ_G, such that the effective strain gradient η that appears in equation $(8)_2$ can be defined as follows:

$$\eta = \frac{\rho_G b}{\bar{r}} \tag{10}$$

The constant $\bar{r} \approx 2$ is the Nye's factor introduced by Arsenlis and Parks (1999) to reflect the scalar measure of GND density resultant from mesoscopic plastic strain gradients.

Now, substituting ρ_S from equation (9) and ρ_G from equation (10) into equation (6) and then in equation (4), and comparing the result with equation $(8)_1$ after substituting equation $(8)_2$ yields the following expression for the intrinsic material length scale ℓ in term of the mean free path of dislocations or the mean spacing between dislocations, L_S, such that:

$$\ell = \hbar L_S \text{ with } \hbar = \bar{r}/m \tag{11}$$

which also gives σ_{ref} as:

$$\sigma_{ref} = G\sqrt{\alpha^2 m^3 b / L_S} \tag{12}$$

The micro-structural length scale parameter, ℓ, and the phenomenological measure of the yield stress in uniaxial tension, σ_{ref}, are now related to measurable physical parameters. It appears from equation $(11)_1$ that the size effect and its implications on the flow stress and work-hardening is fundamentally controlled by the dislocation glide, which is deformation dependent. If one assumes $m \approx 2$ and $\bar{r} \approx 2$ then $\ell \approx L_S$, which can be experimentally measured. Therefore, L_S is a crucial physical measure that controls the evolution of the length scale in gradient plasticity theory for metals such that the key feature of plastic deformation is the reduction of the free path, cell size, or spacing between dislocations with strain.

Moreover, by substituting L_S from equation $(11)_1$ into equation (12), one obtains a relation for ℓ as a function of the shear modulus, yield stress, and other micro-structural parameters, such that:

$$\ell = m^2 \alpha^2 \bar{r} \left(G / \sigma_{ref} \right)^2 b \tag{13}$$

If one sets $m = 3.08$, $\alpha = 0.3$, $b = 0.225\,\text{nm}$, $G/\sigma_{ref} = 100$, then $\ell = 3.8\,\mu\text{m}$ which is a physically sound value in the range of micrometres as reported by many authors in the material community (e.g., Begley and Hutchinson, 1998; Nix and Gao, 1998; Stolken and Evans, 1998; Yuan and Chen, 2001; Zhao et al., 2003; Abu Al-Rub and Voyiadjis, 2004a, 2004b).

3 Model for the hardness indentation size effect

Conical or pyramidal indents whose sizes exceed tens of microns generally produce size-independent hardness values in most metals and can be considered as large indents. Smaller indents in the range from submicron to about 10 μm in single crystals or fine-grained polycrystals often display a significant size effect. For example, the hardness inferred from pyramidal indents on the order of 1 μm in width can be two or three times the hardness obtained from an indent that is 10 μm across. A clear understanding of the ISE and its connection with the material strength is especially important in modern applications involving thin films and multi-layers since micro- and nano-indentation are frequently the only means of measuring their mechanical properties.

In this section, a simple analytical model that can be used to predict equivalently both micro- and nano-hardness when using conical or pyramidal (Berkovich and Vickers) indenters is proposed based on the concept of GNDs.

Tabor (1951) showed in his experiments that the elasto-plastic material response in tensile testing could be correlated to the response in conical/pyramidal indentation. The fundamental parameters for indentation tests by conical/pyramidal indenter are (see Figure 1): the force applied to the indenter, P, the residual contact radius of indentation, a_p, the hardness, $H = P/\pi a_p^2$, the permanent indentation depth, h_p, the total indentation depth, h, the plastic zone radius, c_p, and the indenter geometry; i.e., the angle between the surface of the conical indenter and the plane of the surface θ. This angle is related to h_p and a_p by $\tan\theta = h_p / a_p$ (see Figure 1). The unloading process in the indentation experiment is essential for the proper specification of these geometric parameters. Thus, the residual values h_p and a_p should be used as measurable data in the hardness H calculations.

Consider now the indentation by a rigid cone, as shown schematically in Figure 1. One can assume that the density of GNDs is integrated by the geometry of the indenter and the indentation is accommodated by circular loops of GNDs with Burgers vectors normal to the plane of the surface. One can use the simple model of GNDs developed by Stelmashenko et al. (1993), De Guzman et al. (1993), Nix and Gao (1998), Abu Al-Rub and Voyiadjis (2004b) and Abu Al-Rub (2007) to determine the density of GNDs evolved under a conical/pyramidal indenter. As the indenter is forced into the surface of a single crystal, GNDs are required to account for the permanent shape change at the surface. Of course, SSDs, not shown in Figure 1, would also be created and they would contribute to the deformation resistance.

Figure 1 Axisymmetric rigid conical indenter

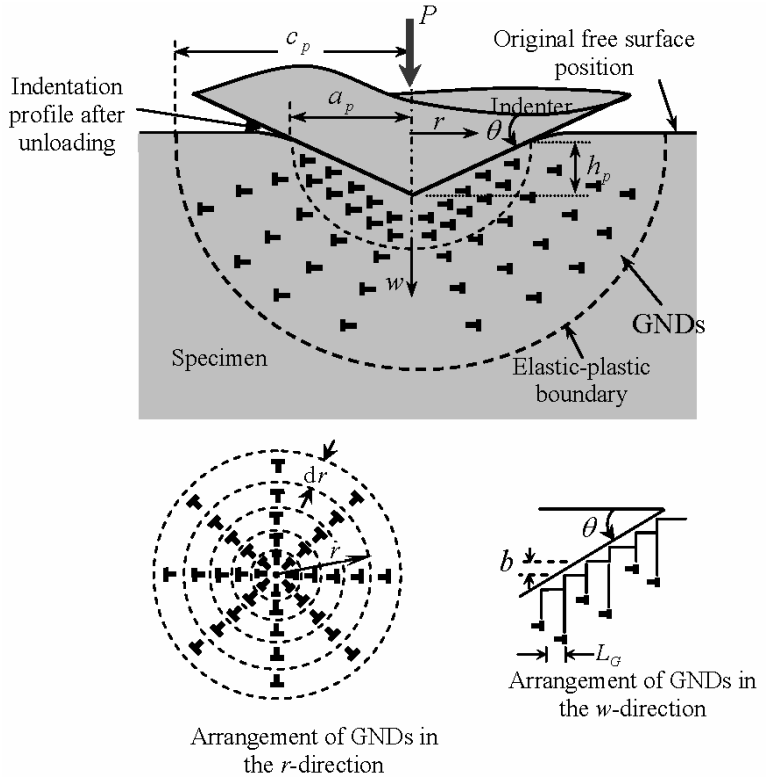

Notes: GNDs created during the indentation process. The dislocation structure is idealised as circular dislocation loops.

The indentation profile in the unloaded configuration when using conical/pyramidal indenters can be described by (see Figure 1):

$$w(r) = h_p - r(\tan\theta) \text{ for } 0 \le r \le a_p \tag{14}$$

It is assumed that the dislocation evolution during indentation is primarily governed by a large hemispherical volume V that scales with the contact radius a_p around the indentation profile (see Figure 1). However, the GNDs reside inside a plasticity zone which can be viewed as extending to a radius c_p to the outermost dislocation emanated from the indent core. Therefore, the size of the plastic zone, c_p, underneath the indenter is larger than the contact radius, a_p, as suggested by Feng and Nix (2004) and Durst et al. (2006) such that $c_p = f\,a_p$ where $f > 1$. Now, one can calculate the GND density using the following relation:

$$\rho_G = \frac{\lambda}{V} \tag{15}$$

where λ is the total length of dislocation loops and V is the storage volume. From Figure 1, one can write:

$$\left|\frac{dw}{dr}\right| = \frac{b}{L_G} = \tan\theta = \frac{h_p}{a_p} \Rightarrow L_G = \frac{ba_p}{h_p} \tag{16}$$

where L_G is the mean spacing between individual slip steps on the indentation surface corresponding to the GND loops. If λ is the total length of the injected loops, then between r and $r + dr$ one can write:

$$\mathrm{d}\lambda = 2\pi r \frac{\mathrm{d}r}{L_G} = 2\pi r \frac{h_p}{ba_p}\mathrm{d}r \tag{17}$$

Integrating from zero to c_p gives the total length of GND loops as:

$$\lambda = \int_o^{c_p} 2\pi r \frac{h_p}{ba_p}\mathrm{d}r = \int_o^{fa_p} 2\pi r \frac{h_p}{ba_p}\mathrm{d}r = \frac{\pi a_p h_p}{b} f^2 \tag{18}$$

One can then assume that all the injected GND loops remain within a hemispherical volume V of radius c_p, such that:

$$V = \tfrac{2}{3}\pi c_p^3 = \tfrac{2}{3}\pi f^3 a_p^3 \tag{19}$$

Therefore, the density of GNDs from equation (15) becomes:

$$\rho_G = \frac{3}{2fbh_p}\tan^2\theta \tag{20}$$

The GND density is reduced by using a bigger storage volume at small indentation depth. In reality the GND density cannot be very large because of the strong repulsive forces between GNDs which push dislocations to spread beyond the hemisphere at small indentation depth (Swadener et al., 2002).

Tabor (1951) specified the mapping from the $H - h_p$ curve to $\sigma - \varepsilon^p$ curve such that one can express the micro-/nano-hardness as:

$$H = \kappa\sigma = \kappa m\alpha bG\left[\sqrt{\rho_S} + \sqrt{\rho_G}\right] \tag{21}$$

where equations (4)and (6) are used in obtaining the above expression. The parameter κ is the Tabor's factor, which has a value from 2.8 to 3.07. The Tabor's relation (i.e., $H = \kappa\sigma$) has been extensively verified and used by many authors in the literature and therefore, one may indeed take it as a starting point.

Based on the assumption of a self-similar deformation field (Hill et al., 1989; Biwa and Storakers, 1995), it was shown that the displacement is proportional to the indentation depth h_p. Based on this observation, Xue et al. (2002) showed from numerical experiments that the strain field should depend only on the normalised

indentation depth h_p / a_p, such that one may assume that the effective plastic strain ε^p is defined by:

$$\varepsilon^p = c\left(h_p / a_p\right) = c\tan\theta \tag{22}$$

where c is a material constant which has a range from 0.2 to 0.4. It can be noted from equation (22) that the plastic strain is independent of the indentation depth.

Considering equations (9), (11), and (22) yields the following expression for the density of SSDs:

$$\rho_S = \frac{c\bar{r}\tan\theta}{\ell b} \tag{23}$$

The macro-hardness H_o is defined as the hardness that would arise from SSDs alone in the absence of GNDs, that is, the hardness that corresponds to the saturation value where the hardness H does not change as the indentation depth h_p increases, or that predicted by classical plasticity theory, such that one can write from equation (21):

$$H_o = \kappa m\alpha bG\sqrt{\rho_S} \tag{24}$$

Substituting equations (20) and (23) into equation (21) along equation (24), one can obtain the following ISE model:

$$H = H_o\left(1+\sqrt{\frac{h^*}{h_p}}\right) \tag{25}$$

where h^* and H_o are, respectively, given by:

$$h^* = \zeta\ell \text{ with } \zeta = \frac{3}{2fc\bar{r}}\tan\theta \tag{26}$$

$$H_o = \kappa\sigma_{ref}c^{1/n}\left(\tan\theta\right)^{1/n} \tag{27}$$

The parameter h^* is a material parameter that characterises the depth dependence of the hardness and is proportional to the material length scale, ℓ, with a proportionality factor ζ which depends on the indenter geometry θ, and the plastic flow through f, c, and $\bar{r}$. Thus, h^* is a crucial parameter that characterises the ISE and its accurate experimental measure gives values for ℓ on which the ability of the strain gradient plasticity theory to guide the development of small-scale systems depends on. Therefore, micro-/nano-indentation hardness data can be effectively used in calibrating the strain gradient plasticity theory. Furthermore, one can note that equation (27) yields a size-independent and constant value for H_o.

One can obtain the commonly used ISE model of Nix and Gao (1998) simply by assuming a linear coupling between SSD and GND densities as in equation (7) [i.e., by setting $\beta = 2$ in equation (3)] and assuming that all the GNDs are stored in a plastic zone of radius equal to the contact radius a_p (i.e., $f = 1$), such that:

$$\frac{H}{H_o} = \sqrt{1 + \frac{h^*}{h_p}} \tag{28}$$

Moreover, Nix and Gao (1998) suggested that h^* and H_o are dependent and related through $h^* = (81/2)b\alpha^2 \tan^2\theta(G/H_o)^2$. Their relation, thus, gives a similar argument to that of equation (26) which suggests that h^* is dependent on the shape of the indenter as well as on the material property.

The size of the plastic zone, c_p, in equation (19) can be calculated using the following well-established relation (e.g., Johnson, 1970; Kramer et al., 1999; Chiu and Ngan, 2002):

$$c_p = \sqrt{\frac{3P}{2\pi\sigma_y}} \tag{29}$$

Substituting in the above expression $H = P/\pi a_p^2$, which is size-dependent with $H_y = \kappa\sigma_y$ is the hardness due to the initial yield stress σ_y and $c_p = fa_p$ yields the ratio of plastic zone size to contact radius as $f = \sqrt{\frac{3}{2}\kappa H/H_y}$. However, $P/\pi c_p^2$ is observed experimentally to be roughly constant with respect to the indent size (Chiu and Ngan, 2002), and this means that H is roughly constant at $r = c_p$. This suggests that the indentation hardness near the elastic-plastic boundary is already approximately self-similar and is not affected by size dependent events at the indent core. Therefore, at $r = c_p$ one can set $H = H_y$, which gives the factor $f = \sqrt{\frac{3}{2}\kappa}$ such that f is constant. For example, substituting $\kappa = 3$ gives $f = 2.12$, which is in the range of the experimental values reported by Kramer et al. (1999), Feng and Nix (2004) and Durst et al. (2006). Moreover, Feng and Nix (2004) suggested a dependence of f on the indentation depth based on phenomenological aspects and not physical ones.

It is noteworthy that the present interpretation of the ISE is based on the evolution of the GNDs, while from time to time in the literature several important factors in experiments (e.g., interfacial friction, indenter pile-up or sink-in, loading rate, oxidation layer, etc.) have been thought to be responsible for the ISE. However, careful experimental studies by Xue et al. (2002) have excluded these factors from being completely responsible for the ISE.

4 Comparison with experimental data

In this section, comparisons are made between the predictions of the present ISE model in equation (25) and that of Nix-Gao model in equation (28) with several micro- and nano-indentation data from the literature. The experimental data reported by Zhang et al. (2005) on bulk Al and undeformed and prestrained Ni, by Kim et al. (2008) on undeformed and prestrained SCM21 (structural steel), and by Zong et al. (2006) on LIGA Ni, (001)Ni, (001)Ag, and (001)Au are utilised here to conduct this comparison. The experimental hardness data obtained from nano- and micro-indentations using,

respectively, Berkovich and Vickers indenters are plotted in Figures 3(a–k) as the hardness H versus the indentation depth h_p.

All the experiment data used here in validating the proposed model, equation (25), are conducted at room temperature and using a Berkovich or Vickers pyramidal indenters for which the nominal or projected contact area varies as:

$$A_c = 24.5h^2 = \pi a^2 \tag{30}$$

Using this relation together with $\tan\theta = h_p / a_p$ yields:

$$\tan\theta = \sqrt{\frac{\pi}{24.5}} = 0.358 \tag{31}$$

The characteristic form for the ISE presented by equation (25) gives a straight line when the hardness data are plotted as H/H_o versus $1/\sqrt{h}$, the intercept of which is one and the slope is $\sqrt{h^*}$. Taking a square of the slope of this curve gives the parameter h^*. For example, this fitting procedure is presented in Figure 2(a) using equation (25) by plotting the LIGA Ni hardness data of Zong et al. (2006) which yields $h^* = 0.079\,\mu\text{m}$. The macroscopic hardness H = 1.892 GPa is obtained when the hardness curve reaches plateau at large indentation depths [see Figure 3(i)]. It can be seen from Figure 2(a) that the proposed model fits very well both the micro- and nano-indentation hardness data.

Nix and Gao (1998) proposed plotting their model in equation (28) as $(H/H_o)^2$ versus $1/h$, which should result in a straight line with slope h^*. Figure 2(b) fits well only the micro-indentation hardness data with $H_o = 2.279\,\text{GPa}$ and $h^* = 0.369\,\mu\text{m}$, but significantly overestimates the nano-indentation hardness data [see Figure 3(i)].

Figure 2 The fitting procedures for both (a) the present model, equation (25), and (b) the Nix and Gao (1998) model, equation (28) (see online version for colours)

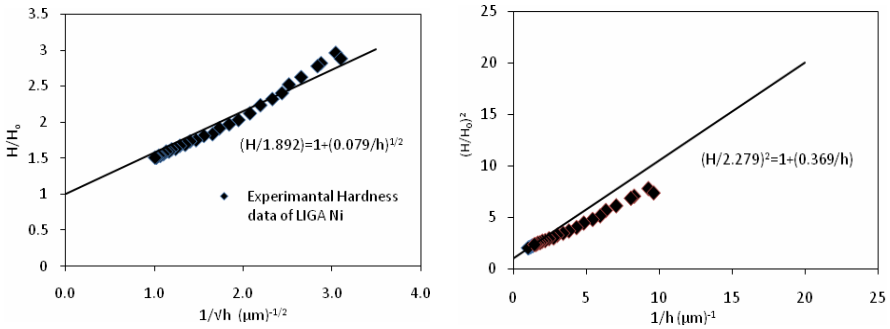

Note: The solid line is a linear curve fit of the experimental hardness results for LIGA Nickel by Zong et al. (2006).

The fitting procedures as described above for both the present model and the Nix-Gao model are repeated for the remaining hardness data of Zhang et al. (2005), Kim et al. (2008) and Zong et al. (2006). In Figures 3(a–l) comparisons between the predictions of the present model, equation (25), and that of the Nix-Gao model, equation (28), are

shown. The values of H_0 and h^* used to fit the experimental results are also shown in the figures.

Figure 3 Comparison of fit of the proposed model and Nix-Gao model to the experimental data: (a) bulk Al (Zhang et al., 2005), (b) undeformed Ni (Kim et al., 2008), (c) 5% prestrained Ni (Kim et al., 2008), (d) 10% prestrained Ni (Kim et al., 2008), (e) 15% prestrained Ni (Kim et al., 2008), (f) undeformed SCM21 (Kim et al., 2008), (g) 2% prestrained SCM21 (Kim et al., 2008), (h) 5% prestrained SCM21 (Kim et al., 2008), (i) LIGA Ni (Zong, 2006), (j) (001) Ni (Zong, 2006), (k) (001) Ag (Zong, 2006) and (l) (001) Au (Zong, 2006)

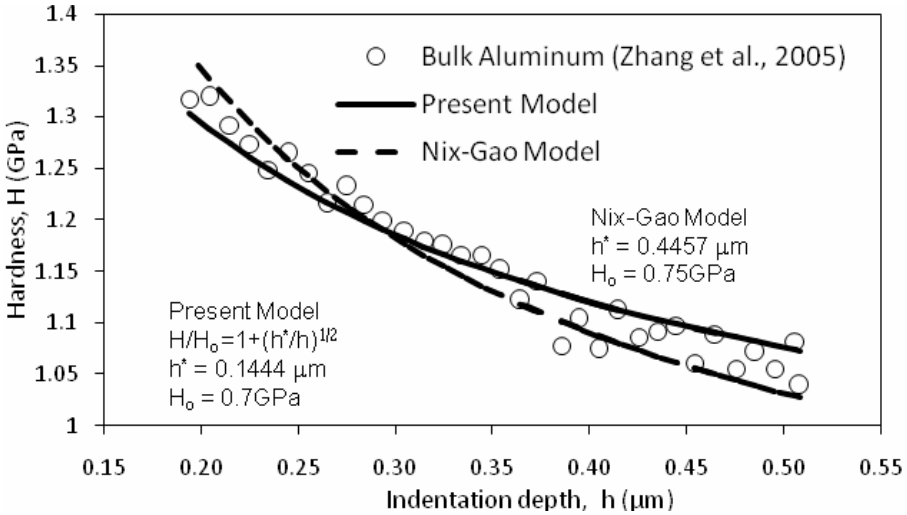

(a)

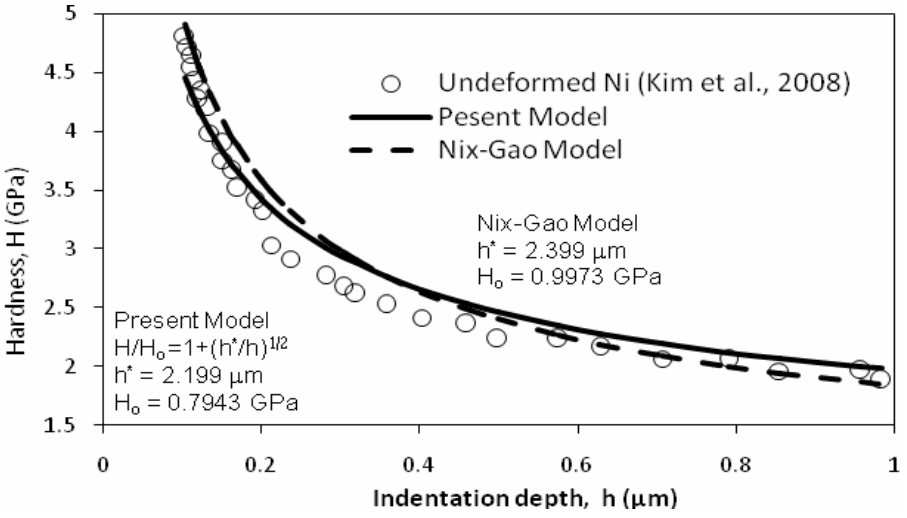

(b)

Note: The symbols Δ and O designate micro-hardness and nano-hardness data, respectively.

Figure 3 Comparison of fit of the proposed model and Nix-Gao model to the experimental data: (a) bulk Al (Zhang et al., 2005), (b) undeformed Ni (Kim et al., 2008), (c) 5% prestrained Ni (Kim et al., 2008), (d) 10% prestrained Ni (Kim et al., 2008), (e) 15% prestrained Ni (Kim et al., 2008), (f) undeformed SCM21 (Kim et al., 2008), (g) 2% prestrained SCM21 (Kim et al., 2008), (h) 5% prestrained SCM21 (Kim et al., 2008), (i) LIGA Ni (Zong, 2006), (j) (001) Ni (Zong, 2006), (k) (001) Ag (Zong, 2006) and (l) (001) Au (Zong, 2006) (continued)

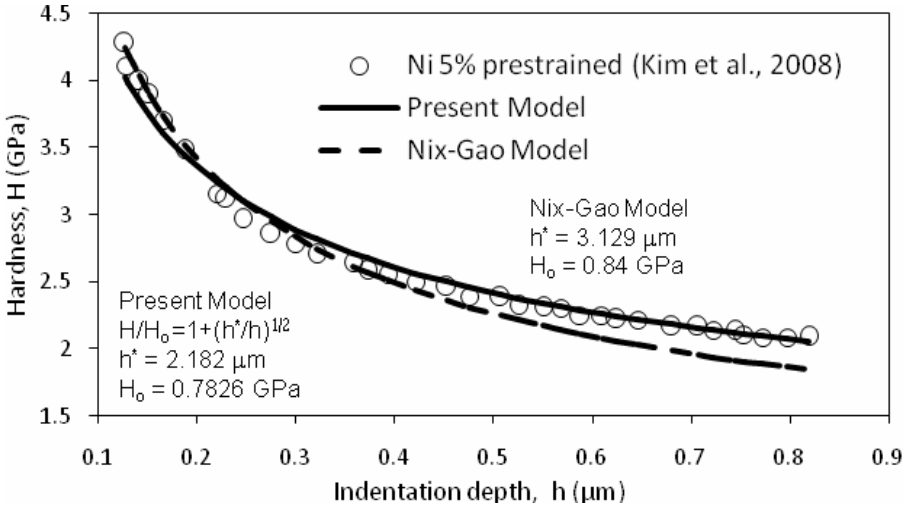

(c)

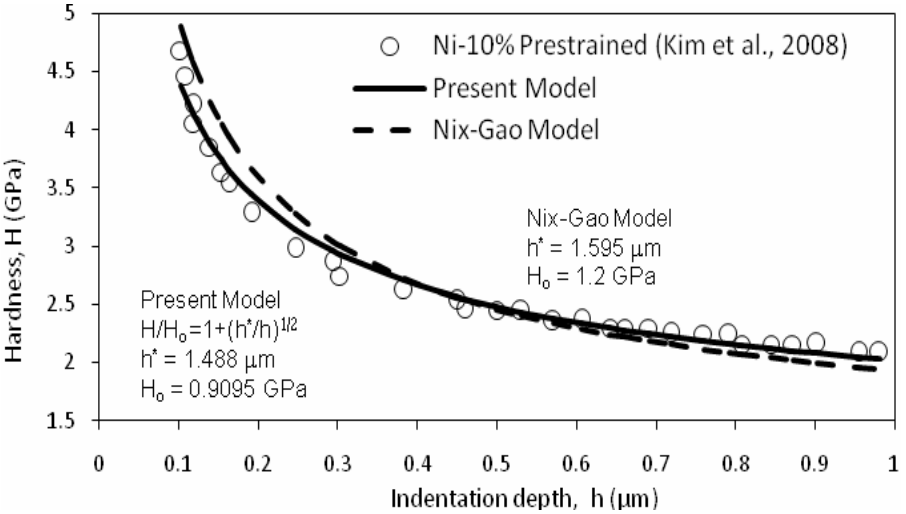

(d)

Note: The symbols Δ and O designate micro-hardness and nano-hardness data, respectively.

Figure 3 Comparison of fit of the proposed model and Nix-Gao model to the experimental data: (a) bulk Al (Zhang et al., 2005), (b) undeformed Ni (Kim et al., 2008), (c) 5% prestrained Ni (Kim et al., 2008), (d) 10% prestrained Ni (Kim et al., 2008), (e) 15% prestrained Ni (Kim et al., 2008), (f) undeformed SCM21 (Kim et al., 2008), (g) 2% prestrained SCM21 (Kim et al., 2008), (h) 5% prestrained SCM21 (Kim et al., 2008), (i) LIGA Ni (Zong, 2006), (j) (001) Ni (Zong, 2006), (k) (001) Ag (Zong, 2006) and (l) (001) Au (Zong, 2006) (continued)

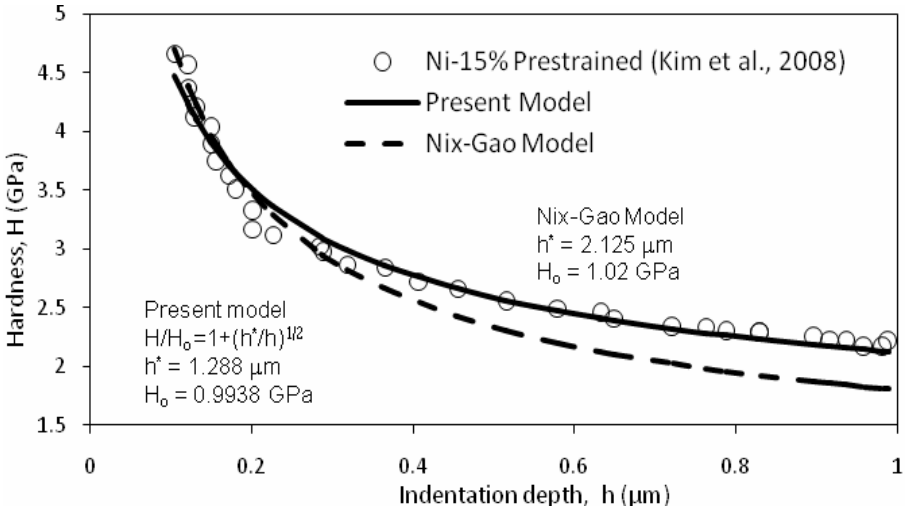

(e)

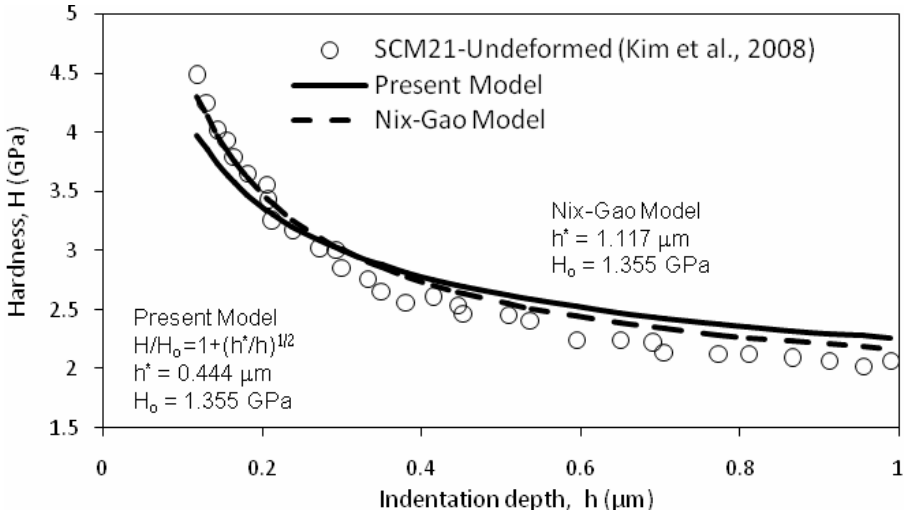

(f)

Note: The symbols Δ and O designate micro-hardness and nano-hardness data, respectively.

Figure 3 Comparison of fit of the proposed model and Nix-Gao model to the experimental data: (a) bulk Al (Zhang et al., 2005), (b) undeformed Ni (Kim et al., 2008), (c) 5% prestrained Ni (Kim et al., 2008), (d) 10% prestrained Ni (Kim et al., 2008), (e) 15% prestrained Ni (Kim et al., 2008), (f) undeformed SCM21 (Kim et al., 2008), (g) 2% prestrained SCM21 (Kim et al., 2008), (h) 5% prestrained SCM21 (Kim et al., 2008), (i) LIGA Ni (Zong, 2006), (j) (001) Ni (Zong, 2006), (k) (001) Ag (Zong, 2006) and (l) (001) Au (Zong, 2006) (continued)

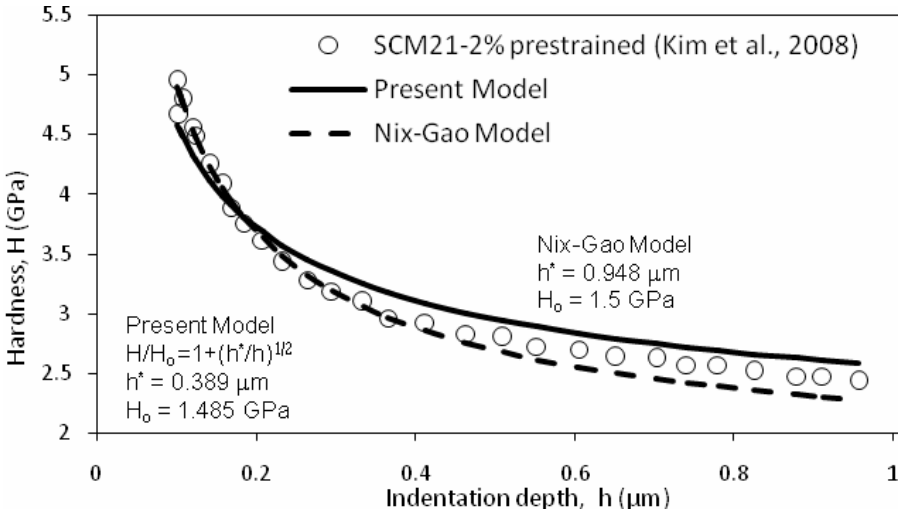

(g)

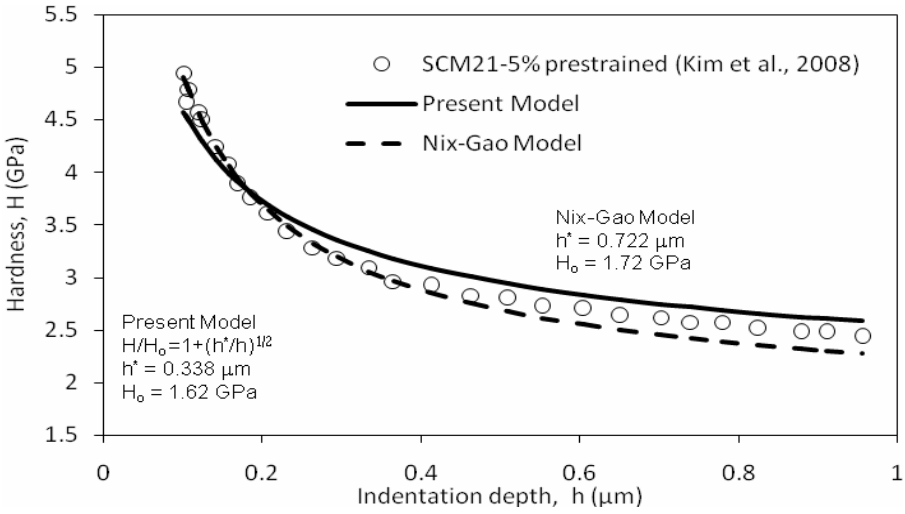

(h)

Note: The symbols Δ and O designate micro-hardness and nano-hardness data, respectively.

Figure 3 Comparison of fit of the proposed model and Nix-Gao model to the experimental data: (a) bulk Al (Zhang et al., 2005), (b) undeformed Ni (Kim et al., 2008), (c) 5% prestrained Ni (Kim et al., 2008), (d) 10% prestrained Ni (Kim et al., 2008), (e) 15% prestrained Ni (Kim et al., 2008), (f) undeformed SCM21 (Kim et al., 2008), (g) 2% prestrained SCM21 (Kim et al., 2008), (h) 5% prestrained SCM21 (Kim et al., 2008), (i) LIGA Ni (Zong, 2006), (j) (001) Ni (Zong, 2006), (k) (001) Ag (Zong, 2006) and (l) (001) Au (Zong, 2006) (continued)

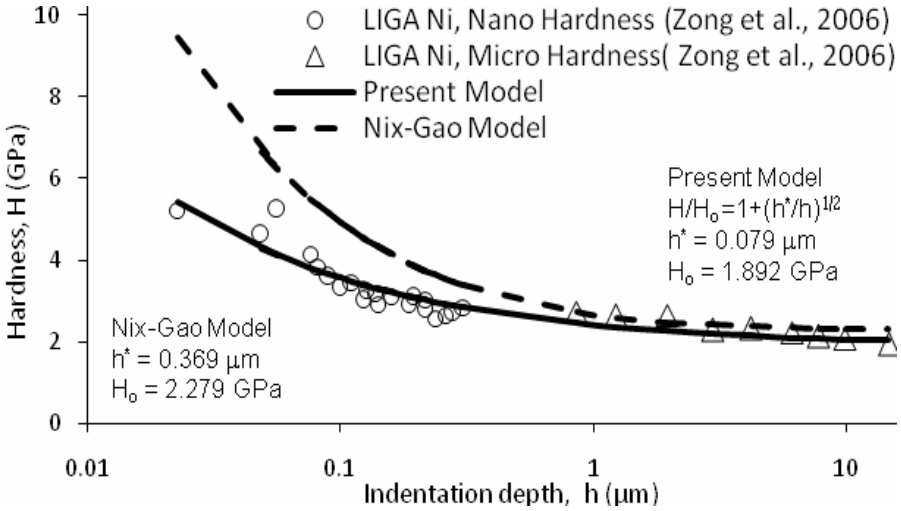

(i)

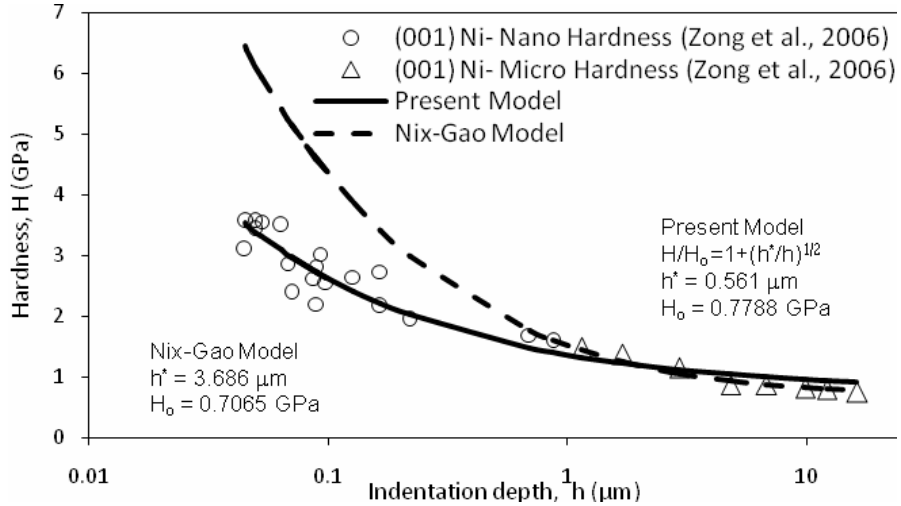

(j)

Note: The symbols Δ and O designate micro-hardness and nano-hardness data, respectively.

Figure 3 Comparison of fit of the proposed model and Nix-Gao model to the experimental data: (a) bulk Al (Zhang et al., 2005), (b) undeformed Ni (Kim et al., 2008), (c) 5% prestrained Ni (Kim et al., 2008), (d) 10% prestrained Ni (Kim et al., 2008), (e) 15% prestrained Ni (Kim et al., 2008), (f) undeformed SCM21 (Kim et al., 2008), (g) 2% prestrained SCM21 (Kim et al., 2008), (h) 5% prestrained SCM21 (Kim et al., 2008), (i) LIGA Ni (Zong, 2006), (j) (001) Ni (Zong, 2006), (k) (001) Ag (Zong, 2006) and (l) (001) Au (Zong, 2006) (continued)

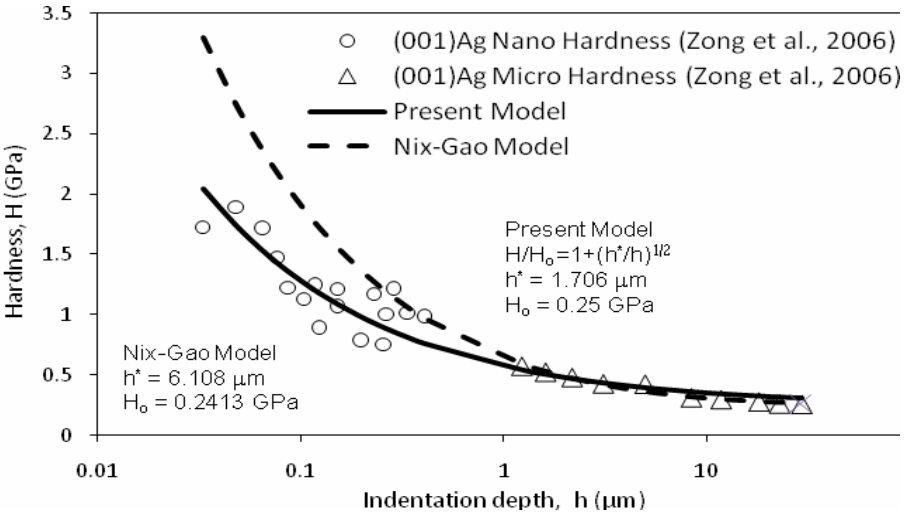

(k)

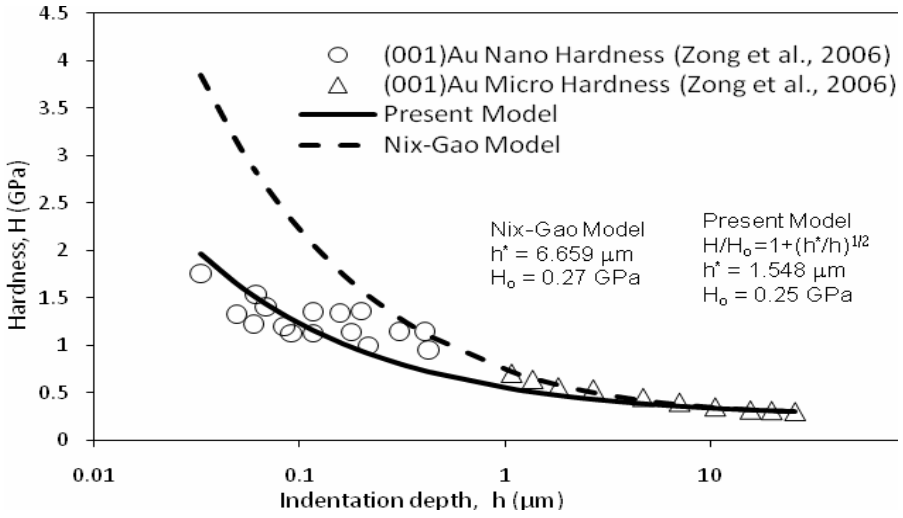

(l)

Note: The symbols Δ and O designate micro-hardness and nano-hardness data, respectively.

A summary of the values for H_o and h^* used to fit the experimental results by the present ISE model in equation (25) is shown in Table 1 along with different parameters of interest obtained from the plotting. The dimensionless parameter $\zeta = 0.633$, which is used to estimate the material length scale parameter, ℓ, is calculated from equation $(26)_2$ by assuming that c = 0.2 [corresponds to 7% effective plastic strain as reported by Johnson (1970) when using pyramidal indentation], the Nye factor $\bar{r} = 2$ (Arsenlis and Parks, 1999), the plastic zone ratio $f = 2.12$ as argued at the end of Section 3, and $\tan\theta = 0.358$. The calculation of ℓ, therefore, strongly depends on the values of the material parameters c, $\bar{r}$, and f. However, as shown in Figure 4 that one of the most important conclusions that one can obtain from the ℓ values for undeformed and prestrained Ni [Figure 4(a)] and SCM21 [Figure 4(b)] in Table 1 is that as the level of prestraining increases the value of ℓ decreases. That is, the value for the material length scale is not fixed or constant for a specific material but depends on the course of deformation and should be considered as an internal variable. This agrees very well with the physical interpretation for ℓ as presented in equation $(11)_1$ which states that the material length scale in metals is related to average spacing between dislocations. Indeed, as the level of prestraining increases, as more dislocations are generated in the microstructure of the material, and as the average spacing between dislocations decreases. Similar arguments have been presented in Abu Al-Rub and Voyiadjis (2004a, 2004b), Voyiadjis and Abu Al-Rub (2005), and Abu Al-Rub (2007) who stated that the length scale parameter is not fixed but decreases as the plastic strain increases. The results in Table 1 confirm their conclusion.

Table 1 The parameters of the present ISE model, equation (25), and the calculation of the length scale parameter ℓ, equation (26), from the fitted hardness data

Material	H_o *(GPa)*	h^* *(μm)*	ζ	$l = h^*/\zeta$ *(μm)*	*ISE*
Bulk Al	0.70 (0.75)	0.1444 (0.4457)	0.633	0.2281	1.202
Undeformed Ni	0.7943 (0.9973)	2.199 (2.399)	0.633	3.474	4.689
5% prestrained Ni	0.7826 (0.84)	2.182 (3.129)	0.633	3.447	4.671
10% prestrained Ni	0.9095 (1.20)	1.488 (1.595)	0.633	2.351	3.857
15% prestrained Ni	0.9938 (1.02)	1.288 (2.125)	0.633	2.035	3.589
Undeformed SCM21	1.355 (1.355)	0.444 (1.117)	0.633	0.701	2.107
2% prestrained SCM21	1.485 (1.50)	0.389 (0.948)	0.633	0.615	1.972
5% prestrained SCM21	1.62 (1.72)	0.338 (0.722)	0.633	0.534	1.838
LIGA Ni	1.892 (2.279)	0.079 (0.369)	0.633	0.125	0.869
(001) Ni	0.7788 (0.7065)	0.561 (3.686)	0.633	0.886	2.368
(001) Ag	0.25 (0.2413)	1.706 (6.108)	0.633	2.695	4.13
(001) Au	0.25 (0.27)	1.548 (6.659)	0.633	2.445	3.934

Note: *The values between brackets are from the Nix-Gao model.

Figure 4 Variation of the length scale parameter value with the level of prestraining for (a) Nickel and (b) SCM21 steel specimens

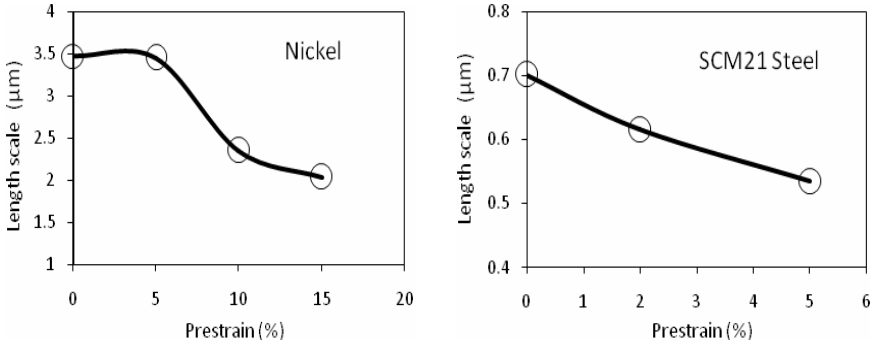

(a) (b)

Source: Kim et al. (2008)

It is noteworthy that the last column in Table 1 presents the ISE index as defined by Abu Al-Rub (2007) such that $\text{ISE} = (H_{0.1} - H_o)/H_o$, where $H_{0.1}$ is the extrapolated nano-hardness at $h = 0.1\mu\text{m}$. This index represents the increase in hardness as compared to the hardness at very large indentation depths (i.e., macro-hardness). A larger value of the ISE index indicates a higher ISE and therefore, it can be used to compare the level of size effect in different materials. Accordingly, it is noticed that the undeformed Ni has the largest ISE and the largest material length scale, followed by 5% prestrained Ni. Thus, it can be generally concluded by comparing the values of the ISE index and the material length scales ℓ in Table 1 that the ISE increases as ℓ increases. Moreover, from the results for undeformed and prestrained Ni and SCM21, one can notice that the level of size effect decreases as the prestrain level increases (or generally as the course of deformation increases).

Using the values listed in Table 2 for the magnitude of the Burgers vector b, the shear modulus G, and the reference stress σ_{ref} from the literature, along with using $m = 3.08$ and $\bar{r} = 2$, one can estimate the coefficient α by using the estimated values for ℓ from its definition in equation (13) which yields reasonable values for α within the correct range (from 0.1 to 0.5). This proves the applicability of equation (13) and the proposed hardness model, equation (26), in identifying the material length scale parameter. Moreover, the last column in Table 2 lists the estimated values for the macro-hardness H_o through using the developed expression in equation (27), where values for the strain-hardening exponent n are obtained from the literature and the Tabor's factor $\kappa = 3$ is used. Close agreement between those estimated values in Table 2 and the corresponding measured values in Table 1 is found.

Figures 3(a–h) are plotted using data analysed from nano-indentation tests only and, as expected, both the models give good predictions of the experimental values. Although it can be noticed that in general, the present model slightly over-predicts the hardness at large indentation depths, because the ISE from the present model does not progressively vanish as fast as the experimental data. This is due to the fact that hardness data at larger indentation depths ($h > 1\mu\text{m}$) should also be measured in order to accurately identify the

macro-hardness value H_o. On the other hand, the Nix-Gao model over-predicts the hardness data at small indentation depths. This is more obvious in Figures 3(i–l).

Table 2 Calculation of the coefficient α and the macro-hardness H_o using equations (13) and (27), respectively

Material	*l (μm)*	*b (nm)*	*G (GPa)*	σ_{ref} *(GPa)*	*α*	*n*	H_o
Bulk Al	0.2281	0.283	27.4	0.39	0.10	10	0.89
Undeformed Ni	3.474	0.25	76	0.864	0.308	2.21	0.786
5% prestrained Ni	3.447	0.25	76	0.601	0.213	4.74	1.034
10% prestrained Ni	2.351	0.25	76	0.542	0.159	8.55	1.195
15% prestrained Ni	2.035	0.25	76	0.512	0.140	16.13	1.304
Undeformed SCM21	0.701	0.248	76.92	0.903	0.143	6.62	1.82
2% prestrained SCM21	0.615	0.248	76.92	0.751	0.112	13.89	1.86
5% prestrained SCM21	0.534	0.248	76.92	0.703	0.10	28.57	1.923
LIGA Ni	0.125	0.25	73	0.81	0.10	19.32	2.12
(001) Ni	0.886	0.25	94.5	0.966	0.14	3.05	1.22
(001) Ag	2.695	0.29	33.6	0.27	0.178	4.92	0.474
(001) Au	2.445	0.29	30.4	0.32	0.222	2.85	0.38

In case of Figures 3(i–l), both micro- and nano-indentation test data are analysed and it can be seen that the present model predictions agree well with both the micro- and nano-hardness data, while the predictions of the Nix-Gao model diverge significantly from the nano-hardness results for $h > 1\,\mu\text{m}$. Moreover, despite the fact that results for indentation depths less than 100 nm are affected by tip rounding, the proposed model fits well both micro- and nano-hardness data although this effect is not considered in formulating the present model. However, it is shown in Huang et al. (2006) that the indenter tip radius effect alone cannot explain the nano-ISE such that the ISE models of Qui et al. (2001), Xue et al. (2002) and Qu et al. (2004), which incorporate this effect, provide only marginal improvements.

Also, from Figures 3(b–h) and Table 1, it is noticed that the ISE is more pronounced in initially undeformed materials whereas the effect gradually reduces if the specimen is prestrained. As in case of nickel, the length scale ℓ reduces from 3.474 μm for undeformed specimen to 2.035 μm for the 15% prestrained specimen and at the same time the ISE index reduces from 4.689 to 3.589 in respective specimens. Similar observation is made in case of structural steel, SCM21, where 2% and 5% prestrained specimens are examined alongside an undeformed one. As discussed above, this can be correlated to the change in the intrinsic material length scale due to the increased initial dislocation density as can be speculated from the physical nature of the length scale being in the order of spacing between dislocations, equation (11). The spacing between dislocations is reduced due to the prestraining and therefore smaller material length scale

and lower ISE is expected, which is confirmed by the experimental results in Figures 3(b–e) and 3(f–h).

Moreover, it can be seen from the values of h^* in Figures 3(a–l) and Table 1 that when using equation (25) for fitting the micro- and nano-indentation hardness data, smaller values for the material length scale parameter are identified than that obtained by the Nix-Gao model. Therefore, it can be concluded that the Nix-Gao model overestimates the length scale parameter whereas the values from the present model are in the order of the spacing between dislocations, which is more physically sound as suggested by equation $(11)_1$.

The proposed ISE model does not account for the indenter tip radius (Xue et al., 2002; Qu et al., 2004) and the indenter pile-up and sink-in (Begley and Hutchinson, 1998; Saha et al., 2001). These effects can be automatically accounted for by using the finite element method for the proposed strain gradient plasticity model in equation (8). This will be the main focus of a future research.

5 Conclusions

In this paper, a dislocation-based ISE model is formulated along the lines of Nix and Gao (1998); however, with one fundamental difference, which is the nature of coupling between SSDs and GNDs in the Taylor's hardening law for metals. In formulating the Nix-Gao ISE model a gross assumption is made such that the total dislocation density is a simple arithmetic sum of SSD and GND densities, whereas in the current model a simple arithmetic sum of the Taylor's stresses from SSD and GND densities is found to be more appropriate and give the correct order of the total dislocation density in hardening metals. This fundamental difference resulted in a new ISE model which corrects the impediment of the Nix-Gao model in overestimating the nano-hardness data such that the present ISE model can fit better both the micro- and nano-hardness data simultaneously. Therefore, one may conclude that *when using the Taylor's hardening law a simple sum of flow stresses from SSDs and GNDs is more adequate than the simple sum of SSD and GND densities.*

Moreover, from dislocation-based arguments it is shown that the material length scale parameter in the strain gradient plasticity theory is not fixed or constant but changes with the course of plastic deformation such that it scales with the average spacing between dislocations. This conclusion is supported by calculating the material length scale parameter from the hardness data of undeformed and prestrained specimens. These data showed that as the prestraining level increases a smaller value for the material length scale is obtained. This suggested that the material length scale should be considered as an internal variable instead of a free parameter.

Finally, it is concluded that materials with smaller length scale are harder and require greater loads in order to create the same contact area, which dictates that the additional amount of hardening during deformation increases as the length scale increases. Thus, the hardest materials have the smallest values of material length scale. It is also concluded that the size effect is more significant in annealed and undeformed specimens than in cold-worked or prestrained or predeformed specimens. This implies that weaker materials exhibit higher ISE. Therefore, the ISE is expected to be influenced by both prior dislocations and the additional work hardening that occurs during indentation.

Acknowledgements

The authors would like to thank US National Science Foundation and the US Department of Energy (NSF#0728032) for their support.

References

Abu Al-Rub, R.K. (2007) 'Prediction of micro and nano-indentation size effect from conical or pyramidal indentation', *Mechanics of Materials*, Vol. 39, pp.787–802

Abu Al-Rub, R.K. and Voyiadjis, G.Z. (2004a) 'Analytical and experimental determination of the material intrinsic length scale of strain gradient plasticity theory from micro- and nano-indentation experiments', *Int. J. Plasticity*, Vol. 20, pp.1139–1182.

Abu Al-Rub, R.K. and Voyiadjis, G.Z. (2004b) 'Determination of the material intrinsic length scale of gradient plasticity theory', *International Journal of Multiscale Computational Engineering,* Vol. 3, No. 3, pp.50–74.

Abu Al-Rub, R.K. and Voyiadjis, G.Z. (2006) 'A physically based gradient plasticity theory', *Int. J. Plasticity,* Vol. 22, pp.654–684.

Alkorta, J., Martinez-Esnaola, J.M. and Gil Sevillano, J. (2006) 'Detailed assessment of indentation size-effect in recrystallized and highly deformed niobium', *Acta Materialia,* Vol. 54, pp.3445–3452.

Arsenlis, A. and Parks, D.M. (1999) 'Crystallographic aspects of geometrically-necessary and statistically-stored dislocation density', *Acta Materialia,* Vol. 47, pp.1597–1611.

Arsenlis, A., Parks, D.M., Becker, R. and Bulatov, V.V. (2004) 'On the evolution of crystallographic dislocation density in non-homogeneously deforming crystals', *J. Mech. Phys. Solids,* Vol. 52, pp.1213–1246.

Ashby, M.F. (1970) 'The deformation of plastically non-homogenous alloys', *Philos. Maga*, Vol. 21, pp.399–424.

Begley, M.R. and Hutchinson, J.W. (1998) 'The mechanics of size-dependent indentation', *J. Mech. Phys. Solids,* Vol. 46, pp.2049–2068.

Biwa, S. and Storakers, B. (1995) 'An analysis of fully plastic Brinell indentation', *J. Mech. Phys. Solids*, Vol. 43, pp.1303–1333.

Busso, E.P., Meissonnier, F.T. and O'Dowd, N.P. (2000) 'Gradient-dependent deformation of two-phase single crystals', *J. Mech. Phys. Solids,* Vol. 48, pp.2333–2361.

Chiu, Y.L. and Ngan, A.H.W. (2002) 'A TEM investigation on indentation plastic zones in Ni3Al(Cr,B) single crystals', *Acta Materialia*, Vol. 50, pp.2677–2691.

De Guzman, M.S., Neubauer, G., Flinn, P. and Nix, W.D. (1993) 'The role of indentation depth on the measured hardness of materials', *Material Research Symposium Proceedings*, Vol. 308, pp.613–618.

Durst, K., Backes, B., Franke, O. and Goken, M. (2006) 'Indentation size effect in metallic materials: modeling strength from pop-in to macroscopic hardness using geometrically necessary dislocations', *Acta Materialia*, Vol. 54, pp.2547–2555.

Elmustafa, A.A. and Stone, D.S. (2002) 'Indentation size effect in polycrystalline F.C.C metals', *Acta Mater*, Vol. 50, pp.3641–3650.

Feng, G. and Nix, W.D. (2004) 'Indentation size effect in MgO', *Scripta Mater*, Vol. 51, pp.599–603.

Fleck, N.A., Muller, G.M., Ashby, M.F. and Hutchinson, J.W. (1994) 'Strain gradient plasticity: theory and experiment', *Acta Metallurgica et Materialia*, Vol. 42, pp.475–487.

Gao, H., Huang, Y., Nix, W.D. and Hutchinson, J.W. (1999) 'Mechanism-based strain gradient plasticity – I. theory', *J. Mech. Phys. Solids*, Vol. 47, pp.1239–1263.

Gerberich, W.W., Tymiak, N.I., Grunlan, J.C., Horstemeyer, M.F. and Baskes, M.I. (2002) 'Interpretation of indentation size effects', ASME Tras., *Journal of Applied Mechanics,* Vol. 69, pp.433–442.

Haque, M.A. and Saif, M.T.A. (2003) 'Strain gradient effect in nanoscale thin films', *Acta Materialia*, Vol. 51, pp.3053–3061.

Hill, R., Storakers, B. and Zdunek, A.B. (1989) 'A theoretical study of the Brinell hardness test', *Proceedings of the Royal Society of London Series A Mathematical Physical and Engineering Sciences*, Vol. 423, No. 1865, pp.301–330.

Huang, Y., Zhang, F., Hwang, K.C., Nix, W.D., Pharr, G.M. and Feng, G. (2006) 'A model of size effects in nano-indentation', *J. Mech. Phys. Solids,* Vol. 54, pp.1668–1686.

Huber, N., Nix, W.D. and Gao, H. (2002) 'Identification of elastic-plastic material parameters from pyramidal indentation of thin films', *Proceedings of the Royal Society of London Series A*, Vol. 458, No. 2023, pp.1593–1620.

Johnson, K.L. (1970) 'The correlation of indentation experiments', *J. Mech. Phys. Solids,* Vol. 18, pp.115–126.

Kim, J.Y., Kang, S.K., Greer, J.R. and Kwon, D. (2008) 'Evaluating plastic flow properties by characterizing indentation size effect using a sharp indenter', *Acta Materialia,* Vol. 56, pp.3338–3343.

Kiser, M.T., Zok, F.W. and Wilkinson, D.S. (1996) 'Plastic flow and fracture of a particulate metal matrix composite', *Acta Mater*, Vol. 44, pp.3465–3476.

Kocks, U.F. (1966) 'A statistical theory of flow stress and work hardening', *Phil. Mag*, Vol. 13, p.541.

Kramer, D., Huang, H., Kriese, M., Rohack, J., Nelson, J., Wright, A., Bahr, D. and Gerberich, W.W. (1999) 'Yield strength predictions from the plastic zone around nanocontacts', *Acta Materialia*, Vol. 47, pp.333–343.

Lim, Y.Y. and Chaudhri, Y.Y. (1999) 'The effect of the indenter load on the nanohardness of ductile metals: an experimental study of polycrystalline work-hardened and annealed oxygen-free copper', *Philoso. Maga,* Vol. A79, No. 12, pp.2979–3000.

Lloyd, D.J. (1994) 'Particle reinforced aluminum and magnesium matrix composites', *Int. Mater. Rev,* Vol. 39, pp.1–23.

Ma, Q. and Clarke, D.R. (1995) 'Size dependent hardness in silver single crystals', *Journal of Materials Research*, Vol. 10, pp.853–863.

Mughrabi, H. (2001) 'On the role of strain gradients and long-range internal stresses in the composite model of crystal plasticity', *Materials Science and Engineering*, Vol. A317, pp.171–180.

Manika, I. and Maniks, J. (2006) 'Size effects in micro- and nano-scale indentation', *Acta Materialia*, Vol. 54, pp.2049–2056.

McElhaney, K.W., Valssak, J.J. and Nix, W.D. (1998) 'Determination of indenter tip geometry and indentation contact area for depth sensing indentation experiments', *Journal of Materials Research,* Vol. 13, pp.1300–1306.

Nan, C-W. and Clarke, D.R. (1996) 'The influence of particle size and particle fracture on the elastic/plastic deformation of metal matrix composites', *Acta Mater*, Vol. 44, pp.3801–3811.

Needleman, A. and Gil Sevillano, J. (2003) 'Preface to the viewpoint set on: geometrically necessary dislocations and size dependent plasticity', *Scripta Materialia*, Vol. 48, No. 2, pp.109–211.

Nix, W.D. and Gao, H. (1998) 'Indentation size effects in crystalline materials: a law for strain gradient plasticity', *J. Mech. Phys. Solids*, Vol. 46, pp.411–425.

Nye, J.F. (1953) 'Some geometrical relations in dislocated crystals', *Acta Metallurgica*, Vol. 1, pp.153–162.

Orowan, E. (1948) *Discussion in Symposium on Internal Stresses in Metals and Alloys*, p.451, Institute of Metals, London.

Poole, W.J., Ashby, M.F. and Fleck, N.A. (1996) 'Micro-hardness of annealed and work-hardened copper polycrystals', *Scripta Materialia*, Vol. 34, pp.559–564.

Qiu, X., Huang, Y., Nix, W.D., Hwang, K.C. and Gao, H. (2001) 'Effect of intrinsic lattice resistance in strain gradient plasticity', *Acta Mater*, Vol. 49, pp.3949–3958.

Qu, S., Huang, Y., Nix, W.D., Jiang, H., Zhang, F. and Hwang, K.C. (2004) 'Indenter tip radius effect on the Nix–Gao relation in micro- and nanoindentation hardness experiments', *J. Mater. Res*, Vol. 19, pp.3423–3434.

Saha, R., Xue, Z., Huang, Y. and Nix, W.D. (2001) 'Indentation of a soft metal film on a hard substrate: strain gradient hardening effects', *J. Mech. Phys. Solids*, Vol. 49, pp.1997–2014.

Shrotriya, P., Allameh, S.M., Lou, J., Buchheit, T. and Soboyejo, W.O. (2003) 'On the measurement of the plasticity length scale parameter in LIGA nickel foils', *Mechanics of Materials*, Vol. 35, pp.233–243.

Stolken, J.S. and Evans, A.G. (1998) 'A microbend test method for measuring the plasticity length-scale', *Acta Mater,* Vol. 46, pp.5109–5115.

Stelmashenko, N.A., Walls, M.G., Brown, L.M. and Milman, Y.V. (1993) 'Microindentation on W and Mo oriented single crystals: an STM study', *Acta Metallurgica et Materialia*, Vol. 41, pp.2855–2865.

Swadener, J.G., George, E.P. and Pharr, G.M. (2002) 'The correlation of the indentation size effect measured with indenters of various shapes', *J. Mech. Phys. Solids*, Vol. 50, pp.681–694.

Tabor, D. (1951) *The Hardness of Metals*, Clarendon Press, Oxford.

Taylor, G.I. (1938) 'Plastic strain in metals', *J. Inst. Metals*, Vol. 62, pp.307–324.

Voyiadjis, G.Z. and Abu Al-Rub, R.K. (2005) 'Gradient plasticity theory with a variable length scale parameter', *International Journal of Solids and Structures*, Vol. 42, pp.3998–4029.

Voyiadjis, G.Z. and Abu Al-Rub, R.K. (2009) *Nonlocal Continuum Damage and Plasticity: Theory and Computation*, World Scientific Publishing Co Pte Ltd., UK.

Xue, Z., Huang, Y., Hwang, K.C. and Li, M. (2002) 'The influence of indenter tip radius on the micro-indentation hardness', *ASME J. Eng. Mater. Technol*, Vol. 124, pp.371–379.

Yuan, H. and Chen, J. (2001) 'Identification of the intrinsic material length in gradient plasticity theory from micro-indentation tests', *Int. J. Solids and Structures*, Vol. 38, pp.8171–8187.

Zhang, F., Saha, R., Huang, Y., Nix, W. D., Hwang, K.C., Qu, S. and Li, M. (2005) 'Indentation of a hard film on a soft substrate: strain gradient hardening effects', *Int. J. Plasticity*, Vol. 23, pp.25–43

Zhao, M., Slaughter, W.S., Li, M. and Mao, S.X. (2003) 'Material-length-scale-controlled nanoindentation size effects due to strain-gradient plasticity', *Acta Materialia*, Vol. 51, pp.4461–4469.

Zong, Z., Lou, J., Adewoye, O.O., Elmustafa, A.A., Hammad, F. and Soboyejo, W.O. (2006) 'Indentation size effect in the nano- and micro-hardness of fcc single crystal metals', *Metarials Science and Engineering*, Vol. A434, pp.178–187.